BMC Pulmonary Medicine

RESEARCH

Open Access

# Assessment of biomechanical properties in pulmonary arterial hypertension: a computational fluid dynamics study of the extensive pulmonary arterial tree

Jian Shi[1†], Jianwen Liang[1†], Jieting Wang[2], Hui Wang[2], Zhenyu Wang[3], Xiaocong Zhang[4], Guifu Wu[1], Shuai Tian[1*] and Wenbin Wei[1*]

## Abstract

Biomechanical forces play a central role in the pathophysiology of pulmonary arterial hypertension (PAH). Due to the numerous branches and complex structure of the pulmonary arteries, three-dimensional reconstruction poses significant challenges, resulting in a lack of comprehensive hemodynamic studies encompassing the entire pulmonary arterial tree in PAH. This study employs computational fluid dynamics (CFD) to evaluate the biomechanical properties of the extensive pulmonary artery tree (segmented up to 6 th-generation branches) in PAH. Key hemodynamic parameters, including velocity, wall shear stress (WSS), time-averaged wall shear stress (TAWSS), oscillatory shear index (OSI), and relative residence time (RRT), were meticulously computed. Results revealed a significant decrease in outlet cross-sectional area ($p < 0.0001$) and a notable increase in outlet velocity compared to the inlet ($p < 0.05$) and main body ($p < 0.001$). WSS in the proximal pulmonary artery was consistently lower than in the distal pulmonary artery for all subjects, with low TAWSS observed in proximal arteries. Helical flow patterns were predominantly seen in proximal pulmonary arteries of PAH subjects. Additionally, high OSI and RRT values were noted within the proximal arteries. This study provides a comprehensive evaluation of hemodynamic parameters in PAH, identifying velocity, WSS, OSI, and RRT as valuable markers of its distinct biomechanical characteristics. These findings shed light on the complex interplay of biomechanical forces in PAH.

**Keywords** Pulmonary artery hypertension, Hemodynamic, Wall shear stress, Oscillatory shear index, Relative residence time

[†]Jian Shi and Jianwen Liang contributed equally to this work and share first authorship.

*Correspondence:
Shuai Tian
tiansh9@mail.sysu.edu.cn
Wenbin Wei
weiwb@mail.sysu.edu.cn
[1] Department of Cardiology, The Eighth Affiliated Hospital, Sun Yat-Sen University, Shenzhen, Guangdong, P.R. China
[2] Department of Cardiac Ultrasound, The Eighth Affiliated Hospital, Sun Yat-Sen University, Shenzhen, Guangdong, P.R. China
[3] Department of Cardiovascular Medicine, Shaanxi Provincial People's Hospital, Xi'an City, Shaanxi Province, People's Republic of China
[4] Department of Cardiology, Foshan Fosun Chancheng Hospital, Foshan, Guangdong, P.R. China

## Introduction

Pulmonary arterial hypertension (PAH) is a chronic disease characterized by a gradual elevation in pulmonary artery pressure. This condition typically ensues from heightened resistance within the distal pulmonary arteries and reduced compliance in the proximal arteries [1, 2]. Individuals diagnosed with PAH face a 5-year survival of 61% [2]. This reduced survival is chiefly attributed to elevated right ventricular afterload, which precipitates the onset of right ventricular failure.

Biomechanical environment within the pulmonary artery plays a pivotal role in maintaining endothelial function. Wall Shear Stress (WSS) plays a critical role in determining the forces exerted on the vessel walls, which is vital in understanding vascular behavior in PAH. It is well-established that both low and high WSS can lead to vascular endothelial dysfunction, a phenomenon that significantly contributes to the pathogenesis and progression of PAH. Oscillatory shear index (OSI) is used to quantify the variation in the direction of the WSS vector, capturing the oscillatory aspect of blood flow. High OSI is associated with disturbed flow patterns, which can contribute to vascular pathologies [3]. In PAH, elevated OSI in certain regions suggests areas of complex flow that may promote disease progression [4]. Relative residence time (RRT) indicates the duration that blood particles spend near the vessel wall [3, 5, 6]. Increased RRT is often observed in PAH, particularly in areas of slow and recirculating flow, which can lead to endothelial dysfunction and vascular remodeling [7]. These indices provide crucial insights into the hemodynamic environment within the pulmonary arteries, aiding in the understanding of disease mechanisms and the development of targeted therapies.

4D-flow MRI provides time-resolved, three-dimensional velocity vector fields of blood flow, enabling a comprehensive analysis of hemodynamic parameters in the pulmonary arteries. Previous investigations using MRI or 4D-flow MRI, have suggested that WSS in the proximal pulmonary artery of PAH patients is lower [8–10]. However, 4D-flow MRI is less effective in characterizing the distal vessels in pulmonary arterial hypertension (PAH). Additionally, 4D-flow MRI requires extended imaging times, involves complex techniques, is costly, and generates intricate data [11]. Furthermore, in patients with pulmonary hypertension (PH), turbulence or slow blood flow can lead to incomplete blood signal suppression, resulting in moderate signal intensity that resembles smoke within the pulmonary artery lumen, thereby causing pulmonary blood flow artifacts [12].

Mathematical models are powerful tools for studying the hemodynamics of distal pulmonary vessels in PAH, offering detailed insights, predictive capabilities. Yang and colleague applied mathematical models in PAH, suggested higher WSS in distal vessels [13]. Since shear stress is a function of velocity, diameter, and curvature, previous mathematical models have not accurately represented the structure of tortuous branches. Although informative, mathematical models often fail to capture the intricate architecture of tortuous arterial branches precisely [14, 15].

Combining computed tomography pulmonary angiography (CTPA) of the entire pulmonary artery tree with CFD helps researchers understand the underlying mechanisms of PAH by studying the complex interactions between blood flow and vascular structures [7, 15]. CTPA provides high-resolution images of the pulmonary arteries, capturing detailed anatomical structures and potential abnormalities. This anatomical information is essential for constructing accurate CFD models. These models use patient-specific anatomical data from CTPA to simulate blood flow dynamics, offering a comprehensive view of both structural (including the proximal and distal parts of the pulmonary artery) and hemodynamic changes in PAH. This approach can lead to new insights into disease progression and identify potential therapeutic targets.

Despite previous investigations into hemodynamics in PAH, there is a scarcity of studies of hemodynamic parameters across the entire pulmonary artery tree of PAH subjects. To gain a deeper understanding of the biomechanical environment in PAH patients, we conducted simulations and meticulously analyzed the biomechanical properties of the entire pulmonary artery tree, encompassing both proximal and distal segments, by integrating CTPA and CFD.

## Methods

### Patient selection

A retrospective study was conducted using clinical data from patients treated at The Eighth Affiliated Hospital, Sun Yat-Sen University in Shenzhen, China, spanning from 2020 to 2022. Inclusion criteria comprised: (1) a diagnosis of idiopathic PAH, (2) availability of complete right heart catheterization (RHC) data, (3) having undergone computed tomography pulmonary angiography with high-quality planar acquisitions suitable for CFD, and (4) possessing a pulmonary blood flow spectrum acquired from echocardiography synchronized with electrocardiography.

In this study, we identified seven PAH patients from the inpatient department aged from 23 to 44, and the diagnosis was confirmed via right heart catheterization following the 2022 ESC/ERS guidelines for pulmonary hypertension. Additionally, a control group of non-PAH subjects was recruited to allow for comparison

of hemodynamic parameters. Non-PAH subjects were selected based on specific inclusion criteria, which ensured they had no history of cardiovascular or pulmonary disease. These subjects underwent the same imaging and simulation procedures as PAH patients for comparative analysis.

### Pre-processing for CFD

CT images with a voxel size of 0.68 ×0.68 ×1.25 mm, encompassing all CT datasets, were imported into Mimics 14.4 (Materialise, Leuven, Belgium) in DICOM format. To determine the contrast window-level ratio, we considered the clarity of contrast between blood vessels and airways. An iterative approach was employed that involved thresholding, region growing, and multiple-slice editing to segment the vasculature in each image dataset, up to the 6th generation of vessels (with the main pulmonary artery designated as generation 0). While this represents a significant advancement over prior studies limited to proximal segments, smaller distal arterioles beyond the 6th generation could not be resolved due to image resolution constraints. The segmentation of further generations was restricted by image resolution.

Arteries were meticulously delineated from veins, a distinction made based on their orientation relative to neighboring airways and their continuity with the main pulmonary artery. Visual inspections ensured proper segmentation of arterial branches.

In this study, the inlet boundary condition was set using a pulsatile velocity profile based on the Womersley profile, derived from the inflow rate measured via echocardiography. It was assumed that the flow at the inlet was fully developed. While this is standard, the main pulmonary artery is relatively short, and the flow jet from the pulmonary valve is unlikely to be perfectly developed.

#### *Segmentation validation and 3D model verification*

To ensure the accuracy of the segmentation and transformation to a 3D model, the following quality control measures were applied:

Segmentation validation: Arteries were carefully delineated from veins based on anatomical location and orientation relative to adjacent airways. Visual inspections ensured the proper segmentation of arterial branches.

3D model verification: A 3D surface representation of the vasculature wasgenerated, followed by smoothing iterations (0–3 iterations) to ensure model accuracy.

Mesh independence testing: Mesh densities were adjusted for each patient's specific anatomy, and results were confirmed to be independent of further mesh refinement.

Next, we generated a 3D surface representation of the patient-specific vasculature from the segmented map, subjecting it to 0–3 iterations of smoothing. Subsequently, we computed a centerline for the vasculature and exported the surface data to 3-Matic (Materialise, Leuven, Belgium). Within 3-Matic, we truncated the domain's inlet and outlets perpendicularly to the centerline. Each inlet and outlet extended approximately 5 times their hydraulic diameter (Dh).

To ensure a fully developed velocity profile, the inlet boundary was extended outward along its normal direction by 5 times the inlet's average radius. Simulations were conducted to confirm that the numerical results were not significantly affected by the length of the inlet extension, ensuring the accuracy and stability of the flow.

At the outlet, a pressure boundary condition was prescribed with a zero pressure assumption, typical for computational models of vascular systems. This condition was applied at the outlet cross-sections to ensure a realistic outflow behavior. Similarly, the inlet and outlet sizes were initially set to 5 times the hydraulic diameter (Dh) to ensure the flow reached a fully developed state before interacting with the rest of the vascular domain (Fig. 1). Although the areas of the inlet and outlet may exhibit slight changes due to the pulsatile nature of blood flow and varying pressure conditions, the inlet and outlet were extended sufficiently to avoid significant impacts on the results of the simulations. This extension was validated through simulations with varying inlet lengths, confirming that the numerical results were stable and not influenced by the inlet extension length.

At the walls, the no-slip condition was applied, assuming that the fluid velocity at the arterial walls was zero, which is standard for modeling vascular flow and for accurately calculating wall shear stress (WSS). These boundary conditions were designed to ensure that the

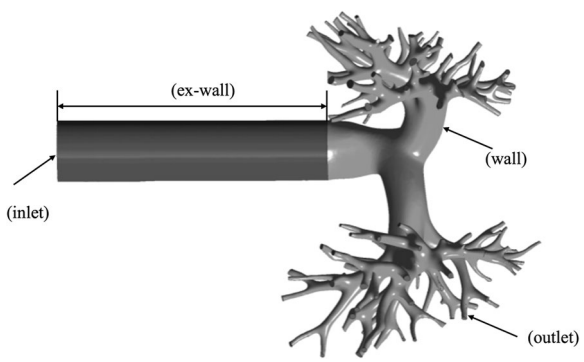


**Fig. 1** Geometry of the pulmonary artery tree from a representative PAH subject (Case P3) with inlet and outlet regions. The inlet and outlet extensions (5 ×hydraulic diameter, Dh) were standardized across all subjects to ensure consistent boundary conditions

simulations accurately capture the hemodynamics of the pulmonary artery system, closely replicating the physiological environment.

### Numerical modeling

The computational domain for the pulmonary system was discretized using unstructured cells, a process facilitated by ICEM-CFD v18.2 (Ansys Inc., Canonsburg, PA). To effectively capture flow behavior in regions with high velocity gradients, we employed boundary inflation layers utilizing the prism cell type. These layers progressively increased in element size from the endoluminal surface towards the core volume. Given the patient-specific variations in size and morphology for each geometry, we adjusted mesh densities accordingly to attain mesh independence. The mesh parameters for each model were defined with allowable edge lengths ranging from 2 mm to 0.1 mm. In this study, approximately 4 million mesh elements were employed for hemodynamic calculations.

To ensure mesh independence, mesh densities were carefully adjusted, and the numerical results were verified to be independent of further mesh refinement. Simulations were conducted using CFX v18.2 (Ansys Inc., Canonsburg, PA) based on a finite-volume method. Given the complexity of the flow, blood was assumed to exhibit Newtonian fluid behavior, with a viscosity of 0.0039 Pas [16] and a density (ρ) of 1060 kg/m$^3$ [17]. This assumption is typically valid in large arteries, where shear rates are high (> 100 s$^{-1}$), minimizing non-Newtonian effects such as shear-thinning. Since our analysis focused on the proximal pulmonary arteries and up to the 6th-generation branches—where shear rates remain elevated—the Newtonian approximation provides a reasonable balance between computational efficiency and physiological accuracy. Gravitational effects were neglected in this study, simplifying the governing transport equations. These equations are the continuity and momentum equations, and they are discretized as Eqs. (1) and (2):

$$\text{Continuity} : \nabla \cdot \vec{U} = 0 \tag{1}$$

$$\text{Momentum} : \rho \frac{\mathrm{D}\vec{U}}{\mathrm{D}t} = -\nabla p + \mu \left( \nabla^2 \vec{U} \right) \tag{2}$$

where $p$ is fluid pressure, $\vec{U}$ is the velocity field.

The simulations were carried out using a transient scheme, with a fixed time-step size of 0.001 s to model the pulsatile nature of blood flow. Two consecutive cardiac cycles were simulated: the first for initialization and the second for analysis. Periodicity was confirmed by the stabilization of key hemodynamic parameters and the convergence of RMS residuals below 10^− 5. A total of two consecutive cardiac cycles were simulated: the first cycle was used to initialize the computational domain, and the results from the second cardiac cycle were used for analysis. This time resolution ensures that the hemodynamic parameters, including velocity, wall shear stress (WSS), and other key metrics, were accurately captured throughout the cardiac cycle. Numerical solutions were obtained when the root mean square (RMS) of both mass and momentum residuals dropped below 10^− 5. Remarkably, even lower RMS residual values were consistently achieved during most time steps. The results of the second cardiac cycle are presented in the following sections.

### Post-processing

WSS represents the dynamic frictional force generated by blood flow along the vascular surface wall [18], and can be calculated as shown in Eq. (3):

$$\overline{\tau} = \mu \dot{\gamma}|_{VascularSurface} \tag{3}$$

TAWSS, which denotes the time-weighted average value of wall shear stress, can be expressed over a single cardiac cycle [19] duration (T) as shown in Eq. (4):

$$\mathrm{TAWSS} = \frac{1}{\mathrm{T}} \int_0^T \left( |\overrightarrow{\tau_w}| \right) \mathrm{dt} \tag{4}$$

OSI quantifies the variation in the direction of the WSS vector, capturing the oscillatory aspect of blood flow [20]. It can be calculated as shown in Eq. (5):

$$\mathrm{OSI} = \frac{1}{2} \left( 1 - \frac{\left| \int_0^T \tau_w dt \right|}{\int_0^T |\tau_w| dt} \right) \tag{5}$$

RRT estimates the proportion of time that blood remains in close proximity to the vessel wall [3], incorporating both TAWSS and OSI. It can be computed as shown in Eq. (6):

$$RRT = \frac{1}{(1 - 2 \times OSI) \times TAWSS} \tag{6}$$

In this study, the computation of the aforementioned hemodynamic factors was carried out using Matlab. Data visualization was performed using CFD-POST and Tecplot.

### Statistics

Statistical comparisons of velocity, area, WSS, TAWSS, OSI, and RRT were performed using Student's t-test for pairwise comparisons and One-way ANOVA for comparisons across multiple groups. Comparisons between PAH and non-PAH subjects were made using Student's

t-test for pairwise comparisons and One-way ANOVA for multiple group comparisons. These methods were chosen to assess the statistical significance of differences between various regions of the pulmonary artery (inlet, main body, and outlet) and to determine whether the observed changes in hemodynamic parameters are significant. A p-value of less than 0.05 was considered statistically significant, ensuring that our findings reflect meaningful differences rather than random variability. Results were considered statistically significant at $p < 0.05$.

## Results

### Subjects' characteristics

Demographic information and clinical evaluations are summarized in Table 1. BSA, body surface area; HR, heart rate; sBP, systolic blood pressure; dBP, diastolic blood pressure; mPAP, mean pulmonary arterial pressure; CO, cardiac output; PAWP, pulmonary artery wedge pressure; PVR, pulmonary vascular resistance.

### The PAH subjects exhibited high outlet velocity and a reduced outlet area

As depicted in Fig. 2(a), the average peak velocities for PAH subjects were 83.9 ± 15.13 cm/s. In comparison, non-PAH subjects exhibited significantly lower peak velocities (average: X ± Y cm/s, reference needed). The average velocities at the inlet, main body, and outlet in PAH subjects were 29.12 ± 4.63 cm/s, 25.79 ± 3.74 cm/s, and 71.54 ± 25.57 cm/s, respectively (Fig. 2b). In contrast, non-PAH subjects showed different velocity patterns, with significantly lower values at the outlet (X ± Y cm/s, $p < 0.05$). These findings indicated a notable increase in velocity at the sub-generation of arteries, with significant differences compared to those at the inlet ($p < 0.05$) and the main body ($p < 0.001$). Conversely, in contrast to the increased velocity, the area at the outlet of the pulmonary artery in PAH subjects (4.64 ± 1.75 $cm^2$) was significantly smaller than at the inlet (9.76 ± 1.45 $cm^2$, $p < 0.0001$) Fig. 2(c). This reduction exceeds normal anatomical tapering and aligns with PAH-associated distal vascular remodeling, as reported in prior studies [2, 15].

**Table 1** Overview of subjects' characteristics

| Subjects | Age | Gender | Weight (kg) | Height (cm) | BSA (m2) | HR (bpm) | sBP (mmHg) | dBP (mmHg) | mPAP (mmHg) | CO (L/min) | PAWP (mmHg) | PVR (WOOD U) |
|---|---|---|---|---|---|---|---|---|---|---|---|---|
| P1 | 36 | Female | 57.5 | 151 | 1.64 | 93 | 113 | 71 | 39 | 3.67 | 2 | 10.08 |
| P2 | 41 | Female | 61 | 151 | 1.64 | 102 | 123 | 80 | 50 | 3.49 | 13 | 10.6 |
| P3 | 44 | Female | 63 | 173 | 1.83 | 58 | 104 | 69 | 48 | 4.38 | 9 | 8.9 |
| P4 | 23 | Female | 52 | 158 | 1.62 | 80 | 94 | 60 | 22 | 4.76 | 2 | 4.2 |
| P5 | 35 | Female | 48.5 | 154 | 1.53 | 58 | 108 | 62 | 57 | 3.22 | 11 | 14.24 |
| P6 | 30 | Female | 60 | 162 | 1.72 | 95 | 101 | 68 | 62 | 3.2 | 5 | 17.81 |
| P7 | 40 | Female | 61 | 158 | 1.71 | 79 | 103 | 73 | 73 | 2.76 | 7 | 23.91 |

*Abbreviations: BSA* Body Surface Area ($m^2$), *HR* Heart Rate (bpm), *sBP* Systolic Blood Pressure (mmHg), *dBP* Diastolic Blood Pressure (mmHg), *mPAP* Mean Pulmonary Arterial Pressure (mmHg), *CO* Cardiac Output (L/min), *PAWP* Pulmonary Artery Wedge Pressure (mmHg), *PVR* Pulmonary Vascular Resistance (Wood Units)

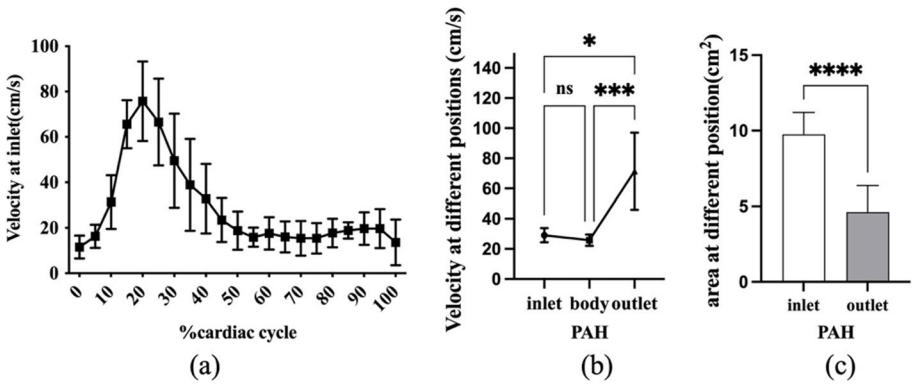


**Fig. 2** Comparison of hemodynamic parameters across the cohort ($n = 7$ PAH subjects). **a** Area-averaged velocity at the inlet over a cardiac cycle. **b** Velocity distribution at inlet, main body, and outlet. **c** Cross-sectional area reduction at the outlet compared to the inlet ($P < 0.0001$). Data are presented as mean ± SD. Note: Asteriks denote statistical significance, with * $P < 0.05$, ** $P < 0.01$, *** $P < 0.001$, **** $P < 0.0001$

### The wall shear stress was notably low in PAH subjects, particularly within the dilated main pulmonary artery

The CFD results revealed that wall shear stress (WSS) varied with changes in the phase of inflow waveform, as depicted in Fig. 3. PAH subjects exhibited larger proximal arteries compared to non-PAH subjects, as shown in Fig. 3(a) and (b). PAH subjects consistently had lower WSS values in the proximal pulmonary artery compared to non-PAH subjects, particularly in the proximal segments. WSS in the proximal pulmonary artery in non-PAH subjects was significantly higher (X ± Y Pa, $p < 0.05$) compared to PAH subjects. Notably, WSS in the proximal pulmonary artery consistently registered lower values than in the distal pulmonary artery throughout the cardiac cycle, a trend observed across all subjects.

The time-averaged wall shear stress (TAWSS) in the extensive pulmonary artery tree (up to 6th-generation branches) of PAH subjects was 2.75 ± 0.98 Pa. At the inlet cross-section, the TAWSS measured 1.00 ± 0.36 Pa for PAH subjects. Meanwhile, at the outlet cross-section, the TAWSS values were 13.35 ± 7.33 Pa for PAH subjects (Fig. 4c). The TAWSS at the outlet cross-section was approximately 13 times higher than that at the inlet cross-section. To understand the influence of specific segments within the pulmonary artery tree, we isolated sections covering the main pulmonary artery trunk, right main pulmonary artery, and left main pulmonary artery, as shown in Fig. 4(b). PAH subjects were found to have significantly lower TAWSS in their proximal arteries (1.02 ± 0.21 Pa) (Fig. 4a). The TAWSS within the main pulmonary artery exhibited a significant decrease compared to both the entire pulmonary artery and its branches (Fig. 4d).

### PAH subjects displayed a greater prevalence of helical flow patterns in the enlarged pulmonary artery during diastole

Streamline images of PAH subjects at peak systole and early diastole were subjected to analysis. The pulmonary artery flow exhibited less helical patterns at peak systole (Fig. 5 a) in comparison to the diastolic phase (Fig. 5 b). Notably, during diastole, several helical flow patterns emerged, extending from the pulmonary artery trunk to its various branches. Furthermore, a greater presence of helical flow was observed in the pulmonary artery trunk, right main pulmonary artery, left main pulmonary artery, and the enlarged pulmonary artery branches within PAH subjects.

### OSI exhibited high values in the dilated pulmonary arteries of PAH subjects

OSI exhibited high values in the dilated pulmonary arteries of PAH subjects, with significantly higher values compared to non-PAH subjects ($p < 0.05$). The distribution of OSI in PAH subjects exhibited notable heterogeneity, with elevated values in regions of vessel dilation, bifurcations, and vascular bends, which were not as pronounced in the non-PAH group. In PAH subjects, OSI values showed significant elevations, especially within the pulmonary artery trunk, right main pulmonary artery, and left main pulmonary artery (Fig. 6). When considering the entire pulmonary artery tree, OSI values averaged 0.041 for PAH subjects. Local OSI values reached up to 0.4 in specific regions of the pulmonary artery (e.g., bifurcations and bends), as visualized in Fig. 6(a-d). However, the average OSI in the proximal arteries was 0.08, and the maximum OSI value recorded in the statistical analysis of the entire cohort was 0.16 (Fig. 6e).

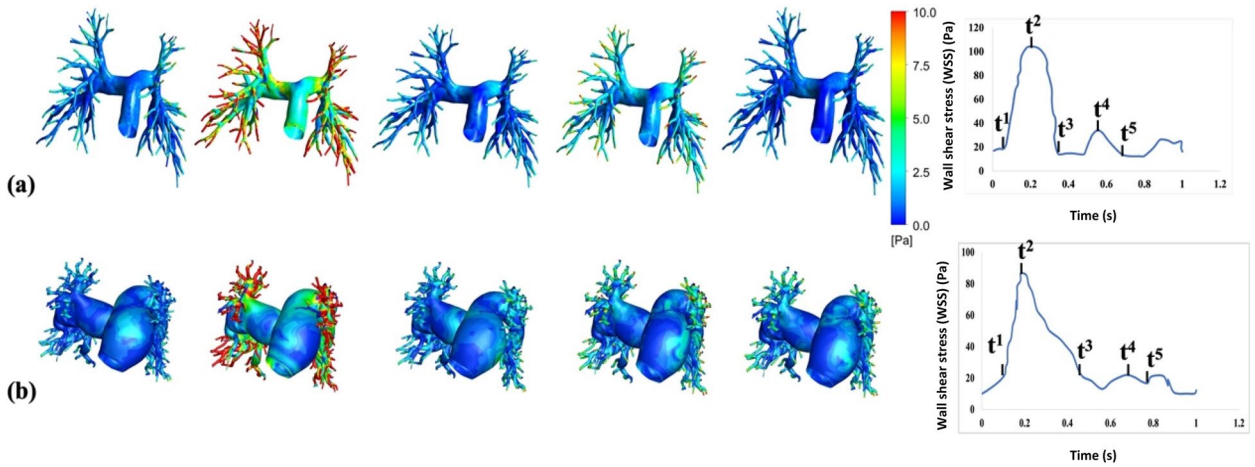


**Fig. 3** Temporal variation of Wall Shear Stress (WSS) in a healthy control (**a**) and a representative PAH subject (Case P3, **b**) at five cardiac phases (t1–t5). The PAH subject exhibits consistently lower WSS in the proximal artery compared to the distal segments

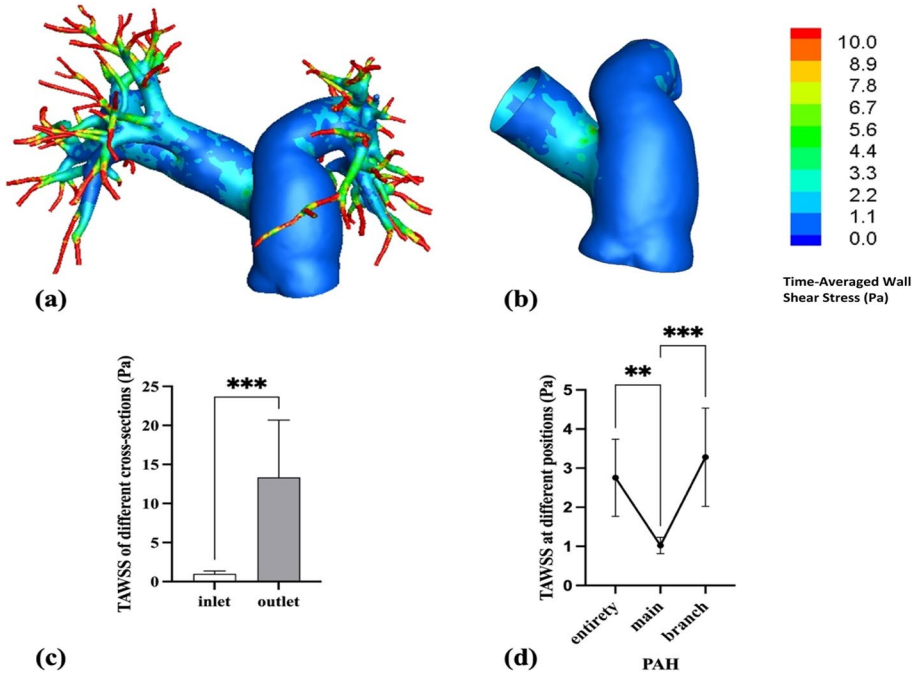


**Fig. 4** Time-averaged WSS (TAWSS) distribution in the pulmonary artery tree of a representative PAH subject (Case P7). **a**, **d** TAWSS across the extensive pulmonary artery tree (up to 6 th-generation branches), main, and branches in PAH subject. **b** Anterior views of proximal arteries. **c** TAWSS at inlet vs. outlet. **d** Comparison of TAWSS in main vs. branch segments. Note: Asteriks denote statistical significance, with * $P < 0.05$, ** $P < 0.01$, *** $P < 0.001$, **** $P < 0.0001$

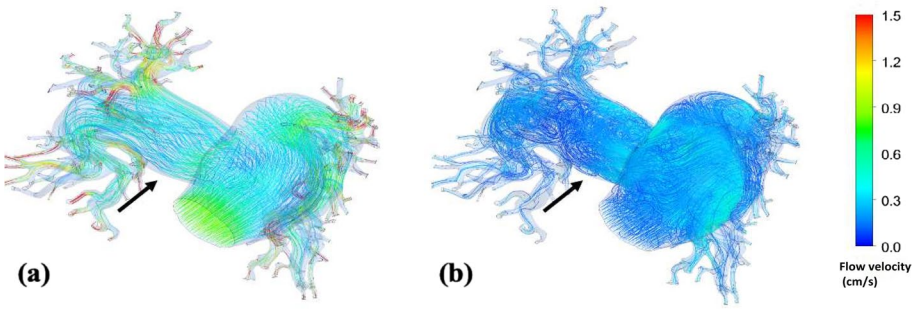


**Fig. 5** Streamline visualization of blood flow in the same PAH subject (Case P5) during peak systole (**a**) and early diastole (**b**). Helical flow patterns (arrows) are more pronounced during diastole, particularly in the dilated proximal arteries. The color map represents flow velocity in [cm/s], with higher velocities indicated by warmer colors and lower velocities by cooler colors. The arrows highlight regions of interest with notable flow patterns

### Relative residence time was high in PAH subjects

Regions characterized by elevated RRT were consistently identified in the main pulmonary artery, at bifurcations, and within vascular bends in PAH subjects, with significantly higher values compared to non-PAH subjects ($p < 0.05$). The median RRT values for non-PAH subjects were significantly lower (X ± Y seconds, $p < 0.05$). (Fig. 7). Areas exhibiting notably high RRT were situated on the anterior wall of dilated pulmonary arteries. The median RRT values for the entire pulmonary artery tree in PAH subjects were 494.1, indicating that blood flow tends to remain in contact with the vessel walls for longer periods, particularly in areas with slower or recirculating flow. Notably, high RRT values (2.00) were observed in the proximal arteries, which are typically dilated in PAH. These regions of slower blood flow and prolonged residence time contribute to endothelial dysfunction and vascular remodeling, which are key features of the disease.

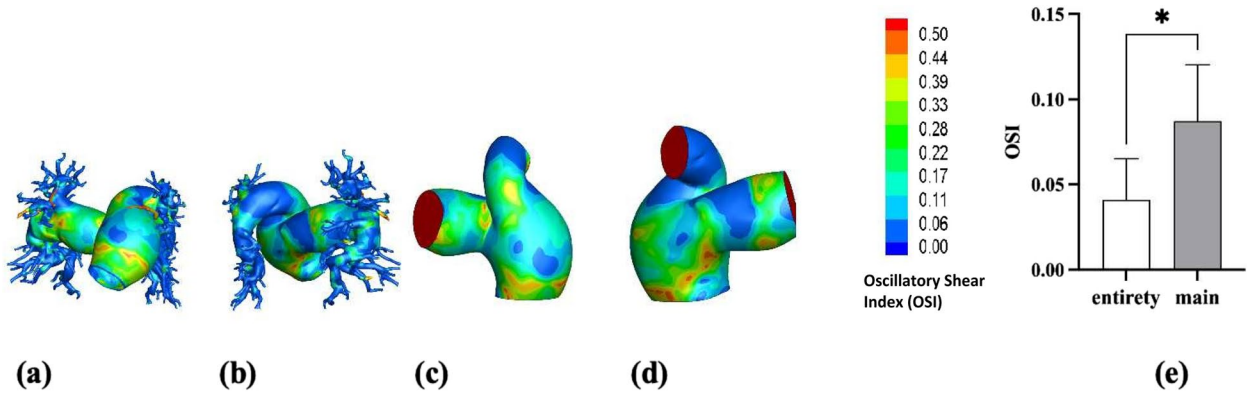


**Fig. 6** Oscillatory Shear Index (OSI) in the representative PAH subject (Case P5). **a**-**b** Anterior/posterior views of the entire arterial tree, highlighting disturbed flow regions (color scale up to OSI = 0.4). **c**-**d** Anterior/posterior views of the main pulmonary artery. **e** Group-averaged OSI ($n = 7$) comparing extensive pulmonary artery tree (up to 6 th-generation branches) and main arteries ($p < 0.05$), with localized peaks reaching OSI = 0.16 in dilated regions. Note: Asteriks denote statistical significance, with * $P < 0.05$, ** $P < 0.01$, *** $P < 0.001$, **** $P < 0.0001$

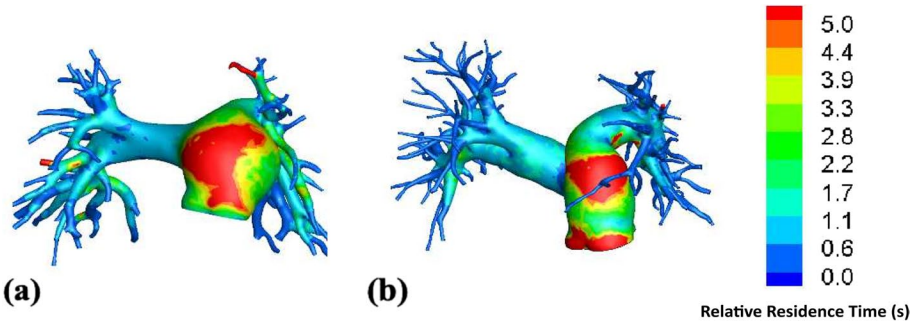


**Fig. 7** Relative Residence Time (RRT) in two PAH subjects (Cases P4 and P7), demonstrating consistent spatial patterns. **a**-**b** 3D visualization cloud images depicting RRT distribution in proximal dilated arteries. **c** Group-averaged RRT values across segments ($p < 0.05$). Data from all subjects ($n = 7$) are shown as median ± standard deviation

## Discussion

PAH is a complex cardiopulmonary disease characterized by obstructive, hyperproliferative vascular lesions, vasoconstriction of pre-capillary arterioles, and sometimes venous obstruction. These factors collectively reduce vessel radius and increase pulmonary vascular resistance (PVR) [2, 21]. Additionally, PAH is marked by the distension and stiffening of proximal vessels, creating a turbulent flow environment in the distal circulation with higher wall shear stress and increased pulse pressures. Due to the numerous branches and complex structure of the pulmonary arteries, three-dimensional reconstruction poses significant challenges, resulting in a lack of comprehensive hemodynamic studies encompassing the extensive pulmonary arterial tree (up to 6 th-generation branches) in PAH. Further research is necessary to thoroughly understand the relationship between the structural changes in the entire pulmonary vasculature and the resulting hemodynamic alterations in PAH. We conducted simulations and meticulously analyzed the biomechanical properties of the extensive pulmonary artery tree (up to 6 th-generation branches), encompassing both proximal and distal segments by integrating CTPA and CFD.

Shear stress and pressure are two crucial biomechanical forces that significantly influence vascular remodeling processes, including wall thickening, dilation, and restenosis [22]. Our findings of reduced WSS and TAWSS in the proximal pulmonary arteries align with prior observations of low shear stress in PAH patients [8, 9]. However, unlike previous MRI-based studies limited to proximal segments [9, 23], our CFD model reveals that TAWSS increases markedly in distal vessels (13.35 Pa at outlets), likely due to the inclusion of 6 th-generation branches. This contrasts with Tang et al. [8], who reported lower distal TAWSS (1.0 Pa) in a truncated arterial tree, underscoring the necessity of whole-tree reconstructions for accurate hemodynamic profiling. The structural changes in pulmonary arteries are also driven by hemodynamic conditions, as seen in compensatory phases of left heart

failure (reduced velocity and shear stress with increased wall tension [24] or congenital heart disease-associated hypertension (elevated cardiac output inducing media thickening [25]. These examples highlight the broader relevance of hemodynamic forces in vascular remodeling. Developing a comprehensive understanding of shear stress patterns throughout the entire pulmonary artery tree is crucial for advancing our knowledge of the pathophysiological mechanisms underlying PAH..

In this study, the area at the outlet of the pulmonary artery in PAH subjects significantly decreased compared to the inlet, corresponding to the pathological changes of reduced distal vessel diameter in PAH. The observed reduction in outlet area, coupled with elevated distal velocity, reflects the pathological interplay between vascular remodeling and hemodynamic stress in PAH. While distal tapering is physiologically expected, the extent of narrowing in PAH exacerbates resistance, amplifying shear stress and oscillatory flow patterns in distal vessels. This magnitude of reduction ($4.64 \pm 1.75$ $cm^2$ vs. $9.76 \pm 1.45$ $cm^2$) exceeds normal anatomical tapering reported in healthy populations [15], aligning with PAH-associated distal arteriolar remodeling driven by medial hypertrophy and intimal fibrosis [2]. Additionally, the study demonstrated a notable increase in velocity at the sub-generation of arteries, with significant differences compared to those at the inlet and main body. Our results demonstrate that distal pulmonary arteries in PAH subjects exhibit increased blood flow velocity, likely due to changes in vascular resistance associated with PAH-induced remodeling. Since vessel diameter and blood flow velocity are key factors in pulmonary artery hemodynamics, the dilation of proximal vessels, narrowing of distal vessels, and increased distal blood flow velocity in PAH can lead to characteristic hemodynamic changes.

The WSS in PAH subjects exhibited fluctuations corresponding to variations in the flow curve, peaking at the maximum flow rate. Importantly, even at peak systole, WSS in the proximal pulmonary arteries remained remarkably low, with a substantial reduction in TAWSS observed in the dilated proximal segments. These localized changes align with the characteristic hemodynamic features of pulmonary hypertension. While earlier studies reported proximal TAWSS values of 0.22–0.43 Pa [8, 9, 26], our results ($1.00 \pm 0.36$ Pa at the inlet) suggest slightly higher baseline shear stress, potentially due to patient-specific variations or methodological differences such as CFD modeling versus 4D-flow MRI [9, 23]. Notably, our data extend these observations by demonstrating that TAWSS disparities between proximal and distal arteries are exacerbated in PAH, correlating with the degree of vascular remodeling. Prior investigations, limited by challenges in peripheral vascular imaging, focused predominantly on proximal segments, leaving reference values for the entire arterial tree poorly defined. Tang et al. [8] reported a distal TAWSS of 1.0 Pa in a truncated arterial tree (4 th-generation reconstruction), whereas our study, incorporating 6 th-generation branches, revealed significantly higher distal TAWSS (13.35 Pa at outlets). This discrepancy underscores the critical impact of comprehensive arterial tree reconstruction on hemodynamic profiling in PAH.

The Oscillatory Shear Index (OSI) serves as a sensitive indicator of disturbed flow, particularly in regions with irregular Wall Shear Stress (WSS), and can contribute to endothelial dysfunction and intimal fibrosis, exacerbating vascular stiffening in PAH patients [27]. It has been suggested that OSI might be especially influenced by irregular flow patterns, such as regurgitation, which are more prevalent in patients with PAH [9]. In our study, higher OSI values were observed in the proximal arteries of PAH subjects, particularly at regions with bifurcations and bends, consistent with disturbed flow patterns. These findings support previous studies that reported elevated OSI in dilated pulmonary arteries of PAH patients. Some studies have also proposed a negative correlation between OSI and WSS [4]. Reiter et al. found that the blood flow vortex in the main pulmonary artery on magnetic resonance imaging (MRI) could assist in diagnosing pulmonary hypertension [28]. Our findings complement previous MRI studies, which reported OSI values in the range of 0.139–0.214 in PAH patients [9, 27]. In contrast, our study revealed a proximal average OSI of 0.08, with localized peaks reaching up to 0.4. While this is consistent with MRI results, CFD offers a critical advantage by allowing for the spatial localization of elevated OSI, particularly in bifurcations and dilated regions (Fig. 6a-d), which MRI's lower resolution may not capture. The spatial specificity of CFD strengthens the link between OSI, endothelial dysfunction, and the progression of PAH. Endothelial cells, as mechanoreceptors, are extremely sensitive to variations in OSI, and previous research has shown a reduction in nitric oxide (NO) production in the endothelial cells of pulmonary arteries in PAH patients [2, 29]. This dysfunction in endothelial cells contributes significantly to peripheral pulmonary arterial vasoconstriction and the advancement of PAH. The increased OSI in dilated regions could inhibit NO production and release, further promoting the pathogenesis of pulmonary arterial hypertension [30, 31].

RRT, a parameter that considers both TAWSS and OSI, emerges as a robust metric for assessing PAH-related alterations. Research on RRT indicates that the extended residence time within recirculation zones offers the requisite exposure duration for activated platelets to adhere to thrombogenic surfaces [32]. In PAH, high RRT values

in the proximal arteries (2.00) are indicative of prolonged blood residence time, which correlates with vessel dilation and altered blood flow dynamics (as depicted in Fig. 7). This extended residence time in these proximal regions may lead to endothelial dysfunction, increased thrombosis risk, and contribute to the vascular remodeling seen in PAH. Our observation of prolonged RRT aligns with histopathological evidence of in-situ thrombosis in PAH [33, 34] and contrasts with abdominal aortic aneurysms, where RRT predicts rupture risk [3]. Notably, PAH-related RRT elevation may guide anticoagulant therapy decisions, a hypothesis warranting clinical validation. These findings underscore RRT's dual role: as a marker of hemodynamic dysfunction in PAH and a potential tool for thrombosis risk stratification.

### Limitations

Studying PAH is particularly challenging due to its rarity. This retrospective study, constrained by the limited number of eligible patients from a single center and stringent inclusion criteria, included only seven cases. While statistical analysis identified distinctive hemodynamic characteristics of PAH, the small cohort size limits its generalizability, and the potential for selection bias inherent in retrospective designs necessitates validation through large-scale prospective studies. Additionally, while our study segmented vessels up to the 6th generation (main pulmonary artery designated as generation 0), the pulmonary arterial tree extends further into smaller arterioles. Image resolution constraints prevented reconstruction of these distal generations, which may exhibit distinct hemodynamic behaviors. Future advancements in imaging and computational power are needed to fully resolve the entire tree. However, the consistency of hemodynamic trends across subjects and their alignment with mechanistic studies [2, 22] supports the validity of our findings. The complex vascular structure of the pulmonary artery significantly influences the hemodynamic environment, requiring further in-depth exploration of its segments. The observed relationship between biomechanical forces and vascular remodeling underscores the need for reliable disease models to advance PAH pathogenesis research.

While our study applied a fully developed velocity profile at the inlet, the main pulmonary artery is short, and the flow jet coming through the pulmonary valve is unlikely to be a perfectly developed parabolic profile. This assumption may introduce inaccuracies, and future studies with patient-specific inlet profiles could refine the modeling of flow behavior. The impact of this idealized inlet condition on the hemodynamic results is acknowledged, and further research would be required to quantify these effects.

## Conclusions

In this study, we conducted 3D hemodynamic simulations of the entire pulmonary artery tree in PAH subjects. We observed the biomechanical environment of the entire pulmonary artery of PAH subjects in detail. PAH subjects exhibited smaller outlet areas and higher outlet velocities when compare with inlet. Additionally, we found lower WSS and TAWSS at the main pulmonary artery in PAH subjects compared to both the entire pulmonary artery and its branches. Furthermore, our analysis revealed the presence of more helical flow, higher OSI, and RRT in the proximal pulmonary artery of PAH subjects. In summary, individuals with PAH exhibited distinct biomechanical characteristics, with velocity, WSS, OSI, and RRT emerging as potent markers for identifying and understanding PAH.

#### Acknowledgements

We thank all the participants in the study.

#### Clinical trial number

Not Applicable.

#### Authors' contributions

J.S., and J.L. performed the conception and design of the study. Data was collected and analyzed by J.W., H.W, Z.W., X.Z., G.W., and S.T. together. Manuscript was drafted by J.S., and J.L. S.T., and W.W. acquired the funding for the study. All authors revised the manuscript and have read and agreed to the publication of the manuscript.

#### Funding

This work was supported by Futian Healthcare Research Project (FTWS2022030) and Shenzhen Science and Technology Program (JCYJ20210324115011030).

#### Data availability

All data generated or analyzed during this study are included in this published article.

## Declarations

#### Ethics approval and consent to participate

The study was conducted following the tenets of the Declaration of Helsinki. The study involved human participants and was approved by the Institutional Review Board of The Eighth Affiliated Hospital, Sun Yat-Sen University, Shenzhen, Guangdong, China (2024ZYKJ073). Since the whole study was a retrospective study, when the data were collected, there was no artificial selection bias due to different groups in the process of patient selection, surgical treatment, and postoperative follow-up observation. Written informed consent was obtained from the patient for participation in this study.

#### Consent for publication

Not Applicable.

#### Competing interests

The authors declare no competing interests.

Received: 15 December 2024 Accepted: 4 April 2025
Published online: 12 April 2025

**References**

1. Humbert M, Kovacs G, Hoeper MM, Badagliacca R, Berger RM, Brida M, Rosenkranz S. 2022 ESC/ERS Guidelines for the diagnosis and treatment of pulmonary hypertension. Eur Respir J. 2022;43(38):3618–731.
2. Thenappan T, Ormiston ML, Ryan JJ, Archer SL. Pulmonary arterial hypertension: pathogenesis and clinical management. BMJ. 2018;360:j5492.
3. Trenti C, Ziegler M, Bjarnegard N, Ebbers T, Lindenberger M, Dyverfeldt P. Wall shear stress and relative residence time as potential risk factors for abdominal aortic aneurysms in males: a 4D flow cardiovascular magnetic resonance case-control study. J Cardiovasc Magn Reson. 2022;24(1):18.
4. Ikoma T, Suwa K, Sano M, Ushio T, Saotome M, Ogawa N, Satoh H, Maekawa Y. Early changes of pulmonary arterial hemodynamics in patients with systemic sclerosis: flow pattern, WSS, and OSI analysis with 4D flow MRI. Eur Radiol. 2021;31(6):4253–63.
5. Chen Z, Yu H, Shi Y, Zhu M, Wang Y, Hu X, Zhang Y, Chang Y, Xu M, Gao W. Vascular Remodelling Relates to an Elevated Oscillatory Shear Index and Relative Residence Time in Spontaneously Hypertensive Rats. Sci Rep. 2017;7(1):2007.
6. Mutlu O, Salman HE, Al-Thani H, El-Menyar A, Qidwai UA, Yalcin HC. How does hemodynamics affect rupture tissue mechanics in abdominal aortic aneurysm: Focus on wall shear stress derived parameters, time-averaged wall shear stress, oscillatory shear index, endothelial cell activation potential, and relative residence time. Comput Biol Med. 2023;154:106609.
7. Kurakula K, Smolders VF, Tura-Ceide O, Jukema JW, Quax PH, Goumans MJ. Endothelial dysfunction in pulmonary hypertension: cause or consequence? Biomedicines. 2021;9(1):57.
8. Tang BT, Pickard SS, Chan FP, Tsao PS, Taylor CA, Feinstein JA. Wall shear stress is decreased in the pulmonary arteries of patients with pulmonary arterial hypertension: An image-based, computational fluid dynamics study'. Pulm Circ. 2012;2(4):470–6.
9. Terada M, Takehara Y, Isoda H, Uto T, Matsunaga M, Alley M. Low WSS and High OSI Measured by 3D Cine PC MRI Reflect High Pulmonary Artery Pressures in Suspected Secondary Pulmonary Arterial Hypertension. Magn Reson Med Sci. 2016;15(2):193–202.
10. Schafer M, Ivy DD, Abman SH, Stenmark K, Browne LP, Barker AJ, Mitchell MB, Morgan GJ, Wilson N, Shah A, Kollengode M, Naresh N, Fonseca B, DiMaria M, Buckner JK, Hunter KS, Kheyfets V, Fenster BE, Truong U. Differences in pulmonary arterial flow hemodynamics between children and adults with pulmonary arterial hypertension as assessed by 4D-flow CMR studies'. Am J Physiol Heart Circ Physiol. 2019;316(5):H1091–104.
11. Marcinno F, Zingaro A, Fumagalli I, Dede L, Vergara C. A Computational Study of Blood Flow Dynamics in the Pulmonary Arteries. Vietnam J Math. 2023;51(1):127–49.
12. Colunga AL, Colebank MJ, Olufsen MS. Parameter inference in a computational model of haemodynamics in pulmonary hypertension. J R Soc Interface. 2023;20(200):20220735.
13. Yang W, Dong M, Rabinovitch M, Chan FP, Marsden AL, Feinstein JA. Evolution of hemodynamic forces in the pulmonary tree with progressively worsening pulmonary arterial hypertension in pediatric patients. Biomech Model Mechanobiol. 2019;18(3):779–96.
14. Walter R, Hunter K, Stenmark K, Kheyfets VO. Hemodynamically Unloading the Distal Pulmonary Circulation in Pulmonary Hypertension: A Modeling Study'. J Biomech Eng. 2022;144(2):024503.
15. Kheyfets VO, Rios L, Smith T, Schroeder T, Mueller J, Murali S, Lasorda D, Zikos A, Spotti J, Reilly JJ, Finol EA. Patient-specific computational modeling of blood flow in the pulmonary arterial circulation. Comput Methods Programs Biomed. 2015;120(2):88–101.
16. Wang Y, Xu L, Chen L, Tong J. Postoperative pulmonary edema and pulmonary hemorrhage following hysteroscopy. BMC Womens Health. 2025;25(1):1–6.
17. Gupta AK, Agrawal SP. Computational modeling and analysis of the hydrodynamic parameters of blood through stenotic artery. Procedia Comput Sci. 2015;1(57):403–10.
18. Soares A, Carvalho F, Leite A. Wall Shear Stress-Based Hemodynamic Descriptors in the Abdominal Aorta Bifurcation: Analysis of a Case Study. J Appl Fluid Mech. 2021;14(6):1657–68.
19. Hoogendoorn A, Kok AM, Hartman EM, de Nisco G, Casadonte L, Chiastra C, Coenen A, Korteland SA, Van der Heiden K, Gijsen FJ, Duncker DJ. Multidirectional wall shear stress promotes advanced coronary plaque development: comparing five shear stress metrics. Cardiovasc Res. 2020;116(6):1136–46.
20. Xu L, Chen X, Cui M, Ren C, Yu H, Gao W, Li D, Zhao W. The improvement of the shear stress and oscillatory shear index of coronary arteries during Enhanced External Counterpulsation in patients with coronary heart disease. PLoS ONE. 2020;15(3):e0230144.
21. Fukumoto Y. Pathophysiology and Treatment of Pulmonary Arterial Hypertension. Int J Mol Sci. 2024;25(2):1166.
22. Lu DY, Chen EY, Wong DJ, Yamamoto K, Protack CD, Williams WT, Assi R, Hall MR, Sadaghianloo N, Dardik A. Vein graft adaptation and fistula maturation in the arterial environment. J Surg Res. 2014;188(1):162–73.
23. Bordones AD, Leroux M, Kheyfets VO, Wu YA, Chen CY, Finol EA. Computational Fluid Dynamics Modeling of the Human Pulmonary Arteries with Experimental Validation. Ann Biomed Eng. 2018;46(9):1309–24.
24. Ben Driss A, Devaux C, Henrion D, Duriez M, Thuillez C, Levy BI, Michel JB. Hemodynamic stresses induce endothelial dysfunction and remodeling of pulmonary artery in experimental compensated heart failure. Circulation. 2000;101(23):2764–70.
25. Mata-Greenwood E, Meyrick B, Steinhorn RH, Fineman JR, Black SM. Alterations in TGF-beta1 expression in lambs with increased pulmonary blood flow and pulmonary hypertension. Am J Physiol Lung Cell Mol Physiol. 2003;285(1):L209–21.
26. Truong U, Fonseca B, Dunning J, Burgett S, Lanning C, Ivy DD, Shandas R, Hunter K, Barker AJ. Wall shear stress measured by phase contrast cardiovascular magnetic resonance in children and adolescents with pulmonary arterial hypertension. J Cardiovasc Magn Reson. 2013;15(1):81.
27. Tiaer M, Ivy DD, Barker AJ, Kheyfets V, Shandas R, Abman SH, Hunter KS, Truong U. Characterization of CMR-derived haemodynamic data in children with pulmonary arterial hypertension. Eur Heart J Cardiovasc Imaging. 2017.
28. Reiter G, Gabor Reiter U, Kovacs F, Bernhard Kovacs G, Kainz F, Karin Kainz B, Schmidt F, Robert Schmidt K, Maier F, Horst Maier R, Olschewski F, Rainer Olschewski H, Rienmueller F, Rienmueller R. Magnetic resonance-derived 3-dimensional blood flow patterns in the main pulmonary artery as a marker of pulmonary hypertension and a measure of elevated mean pulmonary arterial pressure. Circ Cardiovasc Imaging. 2008;1(1):23–30. https://doi.org/10.1161/CIRCIMAGING.108.780247.
29. Tian S, Cai Z, Sen P, van Uden D, van de Kamp E, Thuillet R, Tu L, Guignabert C, Boomars K, Van der Heiden K, Brandt MM, Merkus D. Loss of lung microvascular endothelial Piezo2 expression impairs NO synthesis, induces EndMT, and is associated with pulmonary hypertension. Am J Physiol Heart Circ Physiol. 2022;323(5):H958–74. https://doi.org/10.1152/ajpheart.00220.2022.
30. Malek AM, Izumo S, Alper SL. Modulation by pathophysiological stimuli of the shear stress-induced up-regulation of endothelial nitric oxide synthase expression in endothelial cells. Neurosurgery. 1999;45(2):334–44; discussion 44–5.
31. Malek AM, Jiang L, Lee I, Sessa WC, Izumo S, Alper SL. Induction of nitric oxide synthase mRNA by shear stress requires intracellular calcium and G-protein signals and is modulated by PI 3 kinase. Biochem Biophys Res Commun. 1999;254(1):231–42.
32. Tzirakis K, Kamarianakis Y, Metaxa E, Kontopodis N, Ioannou CV, Papaharilaou Y. A robust approach for exploring hemodynamics and thrombus growth associations in abdominal aortic aneurysms. Med Biol Eng Comput. 2017;55(8):1493–506.
33. Johnson SR, Granton JT, Mehta S. Thrombotic arteriopathy and anticoagulation in pulmonary hypertension. Chest. 2006;130(2):545–52.
34. Johnson SR, Mehta S, Granton JT. Anticoagulation in pulmonary arterial hypertension: a qualitative systematic review. Eur Respir J. 2006;28(5):999–1004.

## Publisher's Note